JOURNAL OF MATERIALS SCIENCE 22 (1987) 2685–2690

Effect of ZrO_2 inclusions on fracture properties of $MgCr_2O_4$

J. P. SINGH
Materials and Components Technology Division, Argonne National Laboratory, Argonne, Illinois 60439, USA

The effects of unstabilized ZrO_2 inclusions on the strength, fracture surface energy and thermal-shock resistance of $MgCr_2O_4$ have been evaluated. The fracture surface energy for $MgCr_2O_4$–ZrO_2 composites was observed to depend on the agglomerate particle size, distribution, and volume fraction of the ZrO_2 inclusions. Large, nonuniformly distributed ZrO_2 inclusions tended to produce a relatively small increase in the fracture surface energy of $MgCr_2O_4$. The fracture surface energy increased with increasing ZrO_2 content to a maximum value of 24.5 J m^{-2} at 16.5 vol% ZrO_2, and decreased as the ZrO_2 content increased further. It is proposed that this four-fold increase in fracture surface energy results from the absorption of energy due to microcrack formation in the $MgCr_2O_4$ matrix, which results primarily from the tensile stresses due to the tetragonal → monoclinic phase transformation of ZrO_2 and the associated volume expansion. The improvement in mechanical properties, specifically the four-fold increase in fracture surface energy, resulted in a substantial increase in thermal-shock resistance of $MgCr_2O_4$–ZrO_2 composites as indicated by the results of thermal-shock experiments.

1. Introduction

Refractory linings for the main pressure vessel of slagging coal gasifiers are subjected to very corrosive environments (molten slag) and to thermal shock caused by the temperature fluctuations [1]. These conditions may result in refractory failure by corrosion, cracking and spalling [2–4]. As indicated by Kennedy [5], refractory degradation by corrosion and thermal shock has been reported in several pilot plants, including the converted Lurgi-type gasifier [6, 7] operated by the British Gas Council and the Bi-Gas pilot plant [8]. In view of the good resistance to corrosion by molten slag, high-chromia refractories (specifically with a $MgCr_2O_4$ spinel phase) appear to be very promising candidates for slagging coal gasifier applications [9–12]. Unfortunately, these high-chromia refractories have relatively poor resistance to thermal-shock fracture [13]. For long service life, these refractories should have good thermal shock as well as corrosion resistance.

The well-known thermal-shock-resistance parameters R'''' and R_{st} [14, 15] are often used to predict the thermal-shock resistance of refractories. These parameters have been derived by Hasselman for a brittle material with uniformly distributed penny-shaped cracks with no crack interactions [16] and are defined as

$$R'''' = \frac{\gamma E}{(1 - \nu)\sigma_f^2} \quad (1)$$

and

$$R_{st} = (\gamma/\alpha^2 E)^{1/2} \quad (2)$$

where γ is the fracture surface energy, E is elastic modulus (Young's modulus of elasticity), ν is Poisson's ratio, σ_f is fracture stress, and α is the coefficient of thermal expansion. The parameter R'''' is proportional to the ratio of the energy required to propagate a crack to the total stored elastic energy at the instant of crack initiation. An increase in the value of R'''' corresponds to a decrease in the final crack length resulting from the propagation of an initially small crack due to thermal shock. On the other hand, R_{st} is proportional to the minimum temperature difference required to initiate the propagation of large cracks under thermal-shock conditions. An increase in the value of R_{st} corresponds to an increase in the critical temperature difference required for fracture initiation for specimens with large cracks. It is clear from Equations 1 and 2 that a high value of the fracture surface energy, γ, will result in improved thermal-shock resistance.

The fracture surface energy, γ, of brittle materials can be improved by incorporating second-phase inclusions. These inclusions may act as crack-arresting sites [17–19] or induce microcracking [20–22] in the matrix which may absorb energy and thus increase the fracture surface energy. Microcracking in the matrix results from the tensile stresses caused by the mismatch between the thermal expansion coefficients, and/or the elastic moduli, of the matrix and the inclusions. An example of the application of expansion coefficient mismatch to cause microcracking and hence improve thermal-shock resistance is the addition of tungsten inclusions in a MgO matrix [23]. The tensile stresses may also include large matrix stresses

0022–2461/87 $03.00 + .12

around inclusions due to the volume change of the inclusions during phase transformation. Microcracking as a result of phase transformation in unstabilized ZrO_2 has been successfully utilized to improve the fracture toughness of Al_2O_3 [20, 21]. Unstabilized ZrO_2 goes through a tetragonal → monoclinic phase change at ~1030° C with an associated linear expansion of ~1.4% [24]. This expansion induces high stresses and associated microcracking at the interface of the ZrO_2 inclusions and the particular matrix, e.g. Al_2O_3, when the material is cooled from the fabrication (sintering, hot pressing) temperature, and results in an increase in fracture surface energy. The purpose of the present study was to evaluate the effect of unstabilized ZrO_2 inclusions on the fracture surface energy of $MgCr_2O_4$–ZrO_2 composites and the resulting improvement in the thermal-shock resistance.

2. Experimental procedure

$MgCr_2O_4$ powder was made by wet ball milling the appropriate amounts of dried $MgCO_3$ and Cr_2O_3 (both laboratory grade, Fisher Scientific Co., Fair Lawn, New Jersey) for 16 h in methanol with Al_2O_3 balls. The slurry mixture was dried in room-temperature air and then calcined at 1200° C for 4 h in air. The structure of the calcined mixture was identified as $MgCr_2O_4$ by X-ray diffraction and the presence of MgO or Cr_2O_3 was not detected. ZrO_2 powders were obtained from two different commercial sources and are designated by ZrO_2-A and ZrO_2-B. As indicated by the X-ray diffraction pattern, ZrO_2-B powder was in the monoclinic form. ZrO_2-A powder primarily consisted of monoclinic phase, and in addition, a weak diffraction line was also present which would be attributed to the presence of a very minor amount of tetragonal/cubic ZrO_2 phase. $MgCr_2O_4$–ZrO_2 composites were made by mixing $MgCr_2O_4$ powder with appropriate amounts of ZrO_2 and then wet ball milling the mixtures for 16 h in methanol with Al_2O_3 balls. The wet mixtures were dried in room-temperature air. The dried mixtures were mixed with 5% acryloid–stearic acid (4:1) binder system dissolved in methanol. Methanol was evaporated from the mixtures by slow heating. The dry mixtures were ground and sieved through a 30-mesh screen. Rectangular bar specimens (~5.1 cm × 0.6 cm × 0.3 cm and 5.1 cm × 0.6 cm × 0.6 cm) of the composites were pressed in a steel die at ~103 MN m^{-2}. These bars were sintered at 1650° C for 1½ h at oxygen partial pressures ranging from ~9 × 10^{-13} to 1 × 10^{-11} atm.

The smaller bars (~5.1 cm × 0.6 cm × 0.3 cm) were used to measure strength in four-point bending with a support span of 3.8 cm, a loading span of 2.2 cm and a cross-head speed of 0.13 cm min^{-1}. The larger bars (~5.1 cm × 0.6 cm × 0.6 cm) were used to measure fracture toughness (critical stress intensity factor, K_{IC}) by the notch beam technique (NBT) [25] with a notch width of ~0.04 cm. The elastic modulus (E) and Poisson's ratio (ν) were measured by the pulse-echo technique [26]. The coefficient of thermal expansion (α) was measured by differential dilatometry. The fracture surface energy (γ) was calculated from the relation $\gamma = K_{IC}^2/2E$ for plane stress conditions. Slightly different values of γ will be obtained from the plane strain relation $\gamma = K_{IC}^2(1 - \nu^2)/2E$. The difference between the two cases will be small for the typical values of Poisson's ratio $\nu \simeq 0.2$ to 0.3. It is also to be noted that plastic deformation in $MgCr_2O_4$ has been assumed to be very limited and γ represents an effective fracture surface energy which includes energy forms other than thermodynamic surface energy.

The thermal-shock resistance of $MgCr_2O_4$ and its composites was measured by quenching rectangular bar specimens (~5.1 cm × 0.6 cm × 0.3 cm) at various temperatures into room temperature silicone oil (Type 200, Dow Corning Corp., Midland, Michigan) with a nominal viscosity of 5 × 10^{-6} m^2 sec^{-1} at 25° C. The specimens were slowly heated to predetermined temperatures in an electrically heated furnace, held at that temperature for ~15 min to attain thermal equilibrium, and dropped into the silicone oil bath. Four specimens were used for each test condition. Mechanical degradation of the specimens was determined by measuring their flexural strength before and after the thermal quench.

3. Results and discussion

3.1. Matrix stresses and critical inclusion size

For microcracking to occur in the $MgCr_2O_4$ matrix around inclusions, the tensile stress in the matrix should exceed the fracture stress for $MgCr_2O_4$ and the particle size of the inclusions should be equal to or greater than a critical value R_c [27]. Following Claussen [20], the tensile stress was estimated by using Selsing's [28] equation for stresses around a spherical particle in an isotropic matrix:

$$\sigma_r = -2\sigma_t = \frac{[-(\alpha_m - \alpha_p)\Delta T](R/r)^3}{[(1 + \nu_m)/2E_m] + [(1 - 2\nu_p)/E_p]} \quad (3)$$

where m and p refer to matrix and inclusion, respectively, σ_r is the radial stress, σ_t is the tangential stress, r is the radial distance from the inclusion, R is the radius of the inclusion, α is the expansion coefficient, ν is Poisson's ratio, E is the elastic modulus, and ΔT is the difference between room temperature and the maximum temperature below which the stresses are no longer relaxed during cooling. To account for the effect of expansion as a result of tetragonal → monoclinic phase transformation, the linear expansion of 1.4% was added in the numerator. The value of ΔT was assumed to be 1000° C. From Equation 3, it can be seen that the maximum σ_t occurs at the interface ($r = R$). From the properties values shown in Table I,

TABLE I Mean properties of ZrO_2 and $MgCr_2O_4$

Property	$MgCr_2O_4$*	Monoclinic ZrO_2
Expansion coefficient, α (10^{-6} °C^{-1})	8.1	7.15†
Elastic modulus, E (GN m^{-2})	159	200
Poisson's ration, ν	0.26	0.29
Surface energy, γ (J m^{-2})	5.9	–

*Present work.
†Value of expansion coefficient taken from [29]; other values assumed.

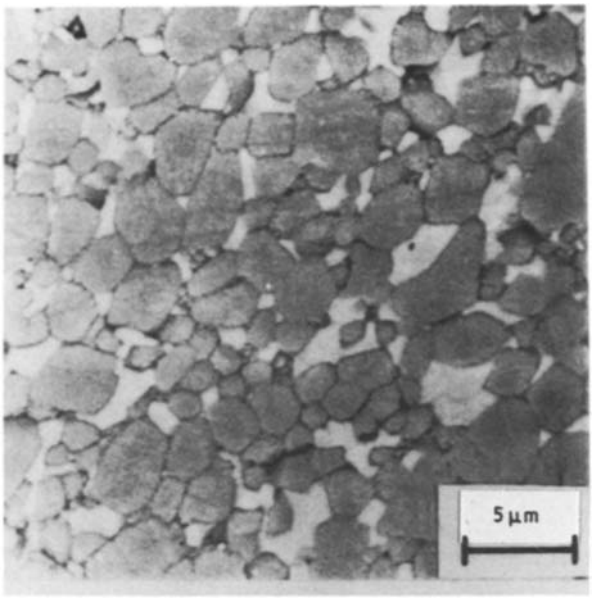

Figure 1 Scanning electron micrograph of a polished and thermally etched specimen of $MgCr_2O_4$–11 vol % ZrO_2-B composite. White areas represent ZrO_2 agglomerates.

the maximum value of σ_t was calculated to be 1229 MN m^{-2} for ZrO_2 inclusions, which is much larger than the fracture stress of the $MgCr_2O_4$ matrix ($\sim$ 66 MN m^{-2}); this result suggests the possibility of microcrack formation in the matrix if ZrO_2 particles are of the critical size. The critical particle size of ZrO_2 inclusions (R_c) for microcrack formation was estimated from the equation proposed by Davidge and Green [27]:

$$R_c \geqslant 8\gamma_s/\{P^2[(1 + \nu_m)/E_m + 2(1 - 2\nu_p)/E_p]\}, \quad (4)$$

where

$$P = \frac{(\alpha_m - \alpha_p)\Delta T}{[(1 + \nu_m)/2E_m] + [(1 - 2\nu_p)/E_p]}$$

and γ_s is the value of fracture surface energy evaluated for the material without inclusions. The other symbols have been defined earlier. Substituting the properties values of Table I in Equation 4, one obtains R_c = 0.6 μm for ZrO_2 inclusions. Preliminary observations of the polished surfaces of $MgCr_2O_4$–ZrO_2 composite indicated that a major portion of the agglomerate ZrO_2 particles were larger than 0.6 μm. These preliminary estimates suggest that the present composite satisfies the conditions of critical stress and inclusion particle size that are required for the occurrence of microcracking in the $MgCr_2O_4$ matrix around the ZrO_2 inclusions.

3.2. Microstructure

The sintered specimens of $MgCr_2O_4$ and $MgCr_2O_4$–ZrO_2-A and -B, composites had densities $\geqslant$ 94 and 96.4% of theoretical value, respectively. (Theoretical densities were calculated by using the rule of mixture. The values assumed for the theoretical densities of $MgCr_2O_4$ and ZrO_2 were 4.42 and 5.6 g cm^{-3}, respectively.) The X-ray diffraction revealed that sintered composites made from both types of ZrO_2 consisted primarily of $MgCr_2O_4$ and monoclinic ZrO_2. In addition, a weak diffraction line was also present which could be attributed to the presence of a very minor amount of tetragonal/cubic ZrO_2 phase. The specimens of $MgCr_2O_4$ and its composites had a fine-grain (grain size < 15 μm) and relatively uniform microstructure. A typical scanning electron micrograph (in back-scatter mode) of polished and thermally etched surface of a $MgCr_2O_4$–11 vol % ZrO_2-B composite is shown in Fig. 1. In the micrograph, the ZrO_2 particles (white regions) are shown to be located intergranularly. Similar grain microstructure was also observed for $MgCr_2O_4$ and $MgCr_2O_4$–ZrO_2-A composites. Fig. 2 shows typical scanning electron micrographs of the fracture surfaces of the specimens of $MgCr_2O_4$ and its composites; a mixed intergranular and transgranular mode of fracture is evident. The fracture surfaces of the composites of $MgCr_2O_4$ with two sources of ZrO_2 (ZrO_2-A and ZrO_2-B) were not observably different and, therefore, only the micrograph of the

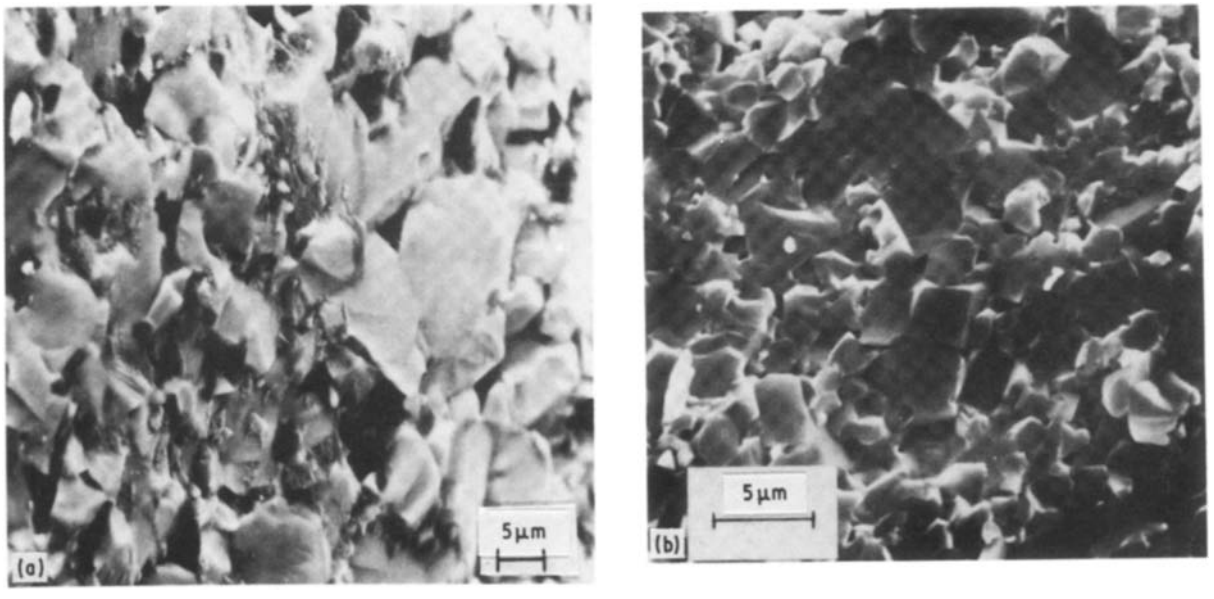

Figure 2 Typical scanning electron micrographs of fracture surface of (a) $MgCr_2O_4$ and (b) $MgCr_2O_4$ + 7% ZrO_2-B composites.

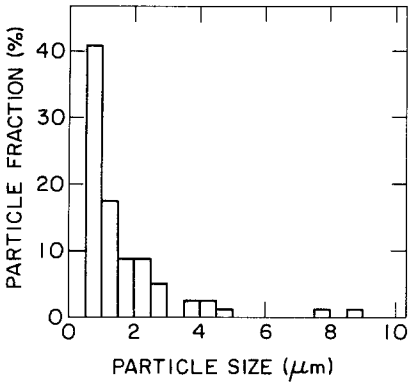

Figure 3 Agglomerate particle size distribution of ZrO_2-A in $MgCr_2O_4$–ZrO_2 composites.

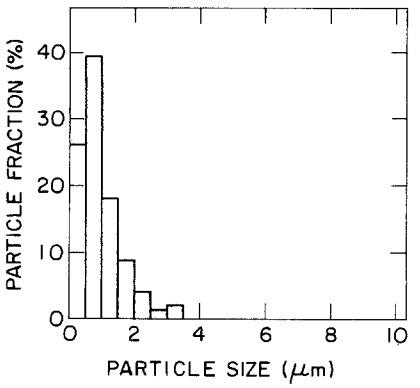

Figure 4 Agglomerate particle size distribution of ZrO_2-B in $MgCr_2O_4$–ZrO_2 composites.

$MgCr_2O_4$–ZrO_2-B composite is shown in Fig. 2. The particle size distribution of the second phase (ZrO_2) was obtained by measuring the agglomerate particle sizes of ZrO_2 on the polished and etched surfaces of the sintered specimens of the $MgCr_2O_4$–ZrO_2 composites. Figs 3 and 4 show the typical size distributions for agglomerate particles of ZrO_2-A and ZrO_2-B, respectively. These figures indicate a difference between the size distributions of ZrO_2 particles for the two types of ZrO_2. The composite specimens with ZrO_2-A (Fig. 3) had a wider distribution of agglomerate particle sizes (0.4 to 9 μm) as compared with the composites with ZrO_2-B (0.2 to 3.5 μm; see Fig. 4). In both cases, the most frequent particle size was $\sim 1\,\mu$m. These distributions suggest that most of the ZrO_2 particles were larger than the critical particle size R_c (0.6 μm) for the formation of microcracks.

3.3. Mechanical properties and thermal-shock behaviour

Table II summarizes the measured values of flexural strength (σ_f), elastic modulus (E), fracture toughness (K_{IC}) and fracture surface energy (γ) as a function of ZrO_2 content for $MgCr_2O_4$–ZrO_2-B composites. For the purpose of comparison, the values of fracture surface energy (γ) for $MgCr_2O_4$–ZrO_2-A composites are also shown in Table II. A plot of the elastic modulus data (Fig. 5) shows that the elastic modulus for $MgCr_2O_4$–ZrO_2-B composites decreases with increasing ZrO_2 content for ZrO_2 contents greater than 7.3%. The decrease in elastic modulus indirectly suggests the existence of microcracking in the $MgCr_2O_4$ matrix, induced by the ZrO_2 inclusions. The initial increase in the elastic modulus value probably derives from the higher elastic modulus of ZrO_2 ($\sim 200\,GN\,m^{-2}$) as compared with that of pure $MgCr_2O_4$ ($\sim 160\,GN\,m^{-2}$) and the very limited initial microcracking.

Fig. 6 shows the dependence of flexural strength (σ_f) and fracture surface energy (γ) (from Table II) on the volume fraction of ZrO_2-B. For the purpose of comparison, the fracture surface energy results for composites with ZrO_2-A are also included in Fig. 6. These results indicate that there is little change in γ for ZrO_2-B contents $\leqslant 7.3\%$, probably because there is little or no microcracking in the matrix for these compositions. At higher ZrO_2 contents, interaction between the stress fields of adjacent ZrO_2 particles may have resulted in a critical stress condition at the matrix–inclusion interface and consequent microcracking of the matrix. The density of microcracks ahead of the notch tip during fracture toughness (K_{IC}) measurements increased with increasing ZrO_2 content; this increase probably resulted in more energy absorption [20, 21] with a corresponding increase in γ. At 16.5% ZrO_2-B content, γ reached a maximum value of $24.5\,J\,m^{-2}$. This represents an approximately four-fold increase in the fracture surface energy of $MgCr_2O_4$ with ZrO_2 inclusions as compared with the value of $MgCr_2O_4$ without any inclusions. Similar improvements have been observed for Al_2O_3 with ZrO_2 inclusions [20, 21]. With a further increase in ZrO_2 content, microcracks begin to join up to form macrocracks;

TABLE II Measured properties of $MgCr_2O_4$–ZrO_2 composite specimens* with different volume fractions of ZrO_2 inclusions

ZrO_2 (vol %)	Flexural strength, σ_f ($MN\,m^{-2}$)	Elastic modulus, E ($GN\,m^{-2}$)	Critical stress intensity factor, K_{IC} ($MN\,m^{-3/2}$)	Fracture surface energy†, γ_{NBT} ($J\,m^{-2}$)	
				with ZrO_2-B	with ZrO_2-A
0	66 ± 7	158 ± 2	1.36 ± 0.05	5.9 ± 0.4	5.9 ± 0.4
3.8	120 ± 15	175 ± 2	1.49 ± 0.06	6.4 ± 0.5	6.4 ± 0.5
7.3	105 ± 15	186 ± 3	1.54 ± 0.02	6.3 ± 0.1	6.9 ± 1.1
10.6	132 ± 11	–	1.79 ± 0.06	8.9 ± 0.6	16.6 ± 2.8
13.6	137 ± 31	174 ± 0	2.26 ± 0.17	14.8 ± 2.2	14.6 ± 0.6
16.5	154 ± 25	166 ± 3	2.84 ± 0.18	24.2 ± 3.0	8.5 ± 2.7
21.6	132 ± 31	166 ± 1	2.42 ± 0.13	17.7 ± 1.9	–

*ZrO_2-B, except as noted.
† γ_{NBT} was calculated from the measured value of K_{IC}.

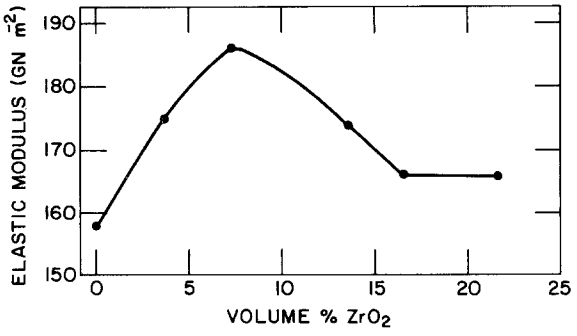

Figure 5 Dependence of elastic modulus on ZrO_2-B content in $MgCr_2O_4$–ZrO_2 composites.

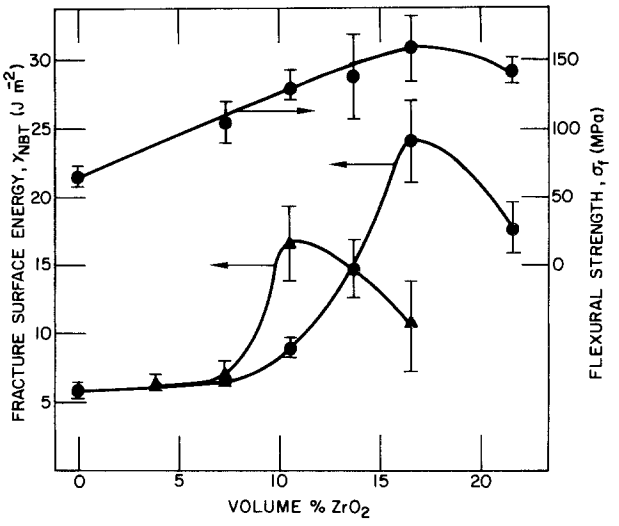

Figure 6 Dependence of strength and fracture surface energy on ZrO_2 content in $MgCr_2O_4$–ZrO_2 composites. (▲) ZrO_2-A, (●) ZrO_2-B.

this process facilitates crack propagation and thus decreases the fracture surface energy. The strength plot in Fig. 6 shows similar trends, i.e. the strength increases with increasing ZrO_2 content, reaches a maximum value of 154 MN m^{-2} at 16.5% ZrO_2-B content, and starts to decrease for ZrO_2-B contents greater than 16.5% because of macrocrack formation. The fracture surface energy (γ) of composites of $MgCr_2O_4$ with ZrO_2-A showed a similar dependence on ZrO_2 content with a maximum γ value of 16.6 J m^{-2} (see Fig. 6). This represents an approximately 2.5-fold increase in γ as compared to a four-fold increase with ZrO_2-B inclusions. This difference is believed to be due to the difference in agglomerate particle size distribution for the two types of ZrO_2 inclusions. The larger nonuniform agglomerates for ZrO_2-A (Fig. 3) may have caused the formation of large nonuniform microcracks, which resulted in lower fracture surface energy as compared to composites with ZrO_2-B inclusions.

It is important to note that at 16.5% ZrO_2-B, the $MgCr_2O_4$–ZrO_2 composites have both high γ and high strength. Similar observations were reported by Becher [21] for Al_2O_3–ZrO_2 composites, but in another study [20], strength was found to decrease as a result of microcracking. The increase in both γ and strength in the present work is proposed to be due to the small size and uniform distribution of the microcracks, which result from the small size and uniform distribution of the ZrO_2 inclusions. As Claussen [20] has also proposed, energy absorption by uniformly distributed small microcracks can increase γ while a small critical crack size is maintained so that the strength is not adversely affected. As indicated before, the composites of $MgCr_2O_4$ with both ZrO_2-A and ZrO_2-B had a very small amount of tetragonal phase. Although the presence of a small amount of tetragonal ZrO_2 may have contributed to some extent to the improvement in mechanical properties of $MgCr_2O_4$–ZrO_2 composites, it is believed that the major part of the improvement is derived from the microcracking.

In view of the four-fold increase in the value of γ for $MgCr_2O_4$ with ZrO_2-B inclusions, $MgCr_2O_4$–ZrO_2-B composites were tested to evaluate the improvements in their thermal-shock resistance.

The results of the thermal-shock experiments are presented in Fig. 7, which shows the retained strength of specimens subjected to varying degrees of thermal quench (ΔT). The results indicate a substantial improvement in the thermal-shock resistance of $MgCr_2O_4$–ZrO_2 composites as compared with pure $MgCr_2O_4$. The value of the critical quenching temperature difference (ΔT_c) for strength degradation due to thermal shock is ~350° C for $MgCr_2O_4$–16.5% ZrO_2 and ~450° C for $MgCr_2O_4$–21.6% ZrO_2, as compared to ~200° C for pure $MgCr_2O_4$. A lower initial strength and higher ΔT_c for $MgCr_2O_4$ + 21.6% ZrO_2 specimens as compared with $MgCr_2O_4$ + 16.5% ZrO_2 specimens is probably due to the presence of larger cracks [14] in $MgCr_2O_4$ + 21.6% ZrO_2 composites. The retained strength after thermal shock for the composite specimens is also higher than that for pure $MgCr_2O_4$.

The results presented above for $MgCr_2O_4$ and its composites with ZrO_2 inclusions clearly indicate that ZrO_2 inclusions substantially improve the mechanical properties (strength and fracture surface energy) of $MgCr_2O_4$ refractories. The extent of improvement will depend upon several parameters such as the particle size and distribution and the amount of inclusion. The improvement in mechanical properties, specifically the four-fold increase in fracture surface energy, has resulted in a substantial increase in thermal-shock resistance of $MgCr_2O_4$–ZrO_2 refractory composites, as shown in Fig. 7. These improvements in mechanical and thermal-shock properties are expected to increase the service life of these refractory composites for slagging coal gasifier applications.

Acknowledgements

The work was supported by the US Department of Energy, Advanced Research and Technology Development Fossil Energy Materials Program, under contract W-31-109-Eng-38. The author thanks R. B. Poeppel, leader of the Ceramics Group, and W. A. Ellingson, Manager of the Fossil Energy Materials Program in the Materials and Components Technology Division for their technical support throughout this work. Thanks are extended to J. J. James

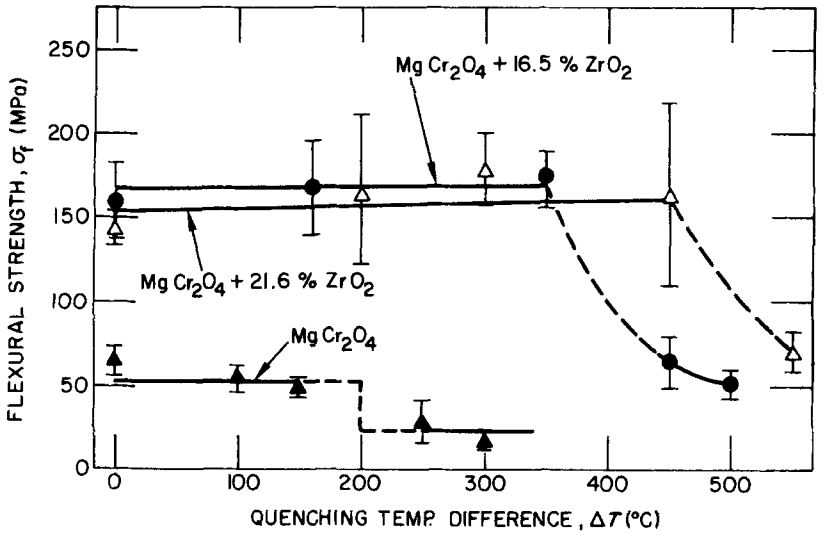

Figure 7 Effect of ZrO_2-B content on thermal-shock behaviour of $MgCr_2O_4$.

and J. J. Picciolo for their valuable experimental assistance.

References

1. W. T. BAKKER, in Proceedings of the 3rd Annual Conference on Materials for Coal Conversion and Utilization, Gaithersburg, MD, CONF-781018, U.S. Department of Energy, Washington, D.C., p. K103 (1978).
2. W. D. KINGERY, *J. Amer. Ceram. Soc.* **38** (1955) 3.
3. B. BRENZY, *Amer. Ceram. Soc. Bull.* **58** (1979) 679.
4. J. NAKAYAMA, in "Fracture Mechanics of Ceramics", Vol. 2, edited by R. C. Bradt, D. P. H. Hasselman and F. F. Lange (Plenum, New York, 1974) p. 759.
5. C. R. KENNEDY, in Proceedings of the 4th Annual Conference on Materials for Coal Conversion and Utilization, Gaithersburg, Maryland, October 1979, CONF-791014, U.S. Department of Energy, Washington, D.C., (1979) p. K60.
6. D. HEBDEN, J. A. LACEY and A. G. HORSLER, *J. Inst. Gas. Eng.* **5** (1965) 367.
7. "Refractories for Coal Gasification and Combustion Systems", EPRI Technical Report AP-1268 (July 1980).
8. "Gas Generator Research and Development: Bi-Gas Process", Phillips Petroleum Company Quarterly Progress Report, January-March 1978, FE-1207-45 (April 1978) p. 127.
9. C. R. KENNEDY and R. B. POEPPEL, *Interceram.* **27** (1978) 221.
10. J. A. BONAR, C. R. KENNEDY and R. B. SWAROOP, *Amer. Ceram. Soc. Bull.* **59** (1980) 473.
11. C. R. KENNEDY, *J. Mater. Energy Syst.* **2** (2) (1980) 11.
12. C. R. KENNEDY, "Refractory/Coal-Slag Compatibility Studies: Progress to Date," presented at the American Ceramics Society Annual Meeting, Washington, D.C. (1981).
13. J. P. SINGH, D. R. DIERCKS, R. B. POEPPEL and G. BANDYOPADHYAY, "Thermal-Shock Studies on Refractories for Slagging Coal Gasifiers," Argonne National Laboratory Report, ANL/FE-84-3 (1984).
14. D. P. H. HASSELMAN, *J. Amer. Ceram. Soc.* **52** (1969) 600.
15. D. P. H. HASSELMAN, Thermal Stress Crack Stability and Propagation in Severe Thermal Environments, in "Materials Science Research", Vol. V, "Ceramics in Severe Environments", edited by W. W. Kriegel and H. Palmour III (Plenum, New York, 1971) p. 89.
16. J. P. SINGH, C. SHIH and D. P. H. HASSELMAN, *Commun. Amer. Ceram. Soc.* **64** (8) (1981) 106.
17. D. P. HASSELMAN and R. M. FULRATH, *J. Amer. Ceram. Soc.* **49** (1966) 68.
18. F. F. LANGE, *Philos. Mag* **22** (1970) 983.
19. DIPAK R. BISWAS and RICHARD M. FULRATH, *J. Amer. Ceram. Soc.* **58** (1975) 526.
20. N. CLAUSSEN, *ibid.* **59** (1976) 49.
21. P. F. BECHER, *ibid.* **64** (1981) 37.
22. N. CLAUSSEN and J. JAHN, *ibid.* **61** (1978) 94.
23. R. C. ROSSI, *Amer. Ceram. Bull.* **48** (1969) 736.
24. R. N. PATIL and E. C. SUBBARAO, *J. Appl. Crystallogr.* **2** (1969) 281.
25. W. F. BROWN Jr. and J. E. SRAWLEY, American Society for Testing and Materials Special Technical Publication no. 410, p. 13 (ASTM, Philadelphia, Pennsylvania, 1966).
26. J. KRAUTKRÄMER and H. KRAUTKRÄMER, "Ultrasonic Testing of Materials" (Springer-Verlag, New York, 1983).
27. R. W. DAVIDGE and T. J. GREEN, *J. Mater. Sci.* **3** (1968) 629.
28. J. SELSING, *J. Amer. Ceram. Soc.* **44** (1961) 419.
29. R. RUH, G. W. HOLLENBERG, S. R. SKAGGS, S. D. STODDARD, F. G. GAC and E. G. CHARLES, *Amer. Ceram. Soc. Bull.* **60** (1981) 504.

Received 25 March 1986
and accepted 15 January 1987